

A COMPARATIVE STUDY OF SATELLITE IMAGE RESOLUTIONS FOR DETECTING PEST DAMAGE IN SUNFLOWER FIELDS

B. S. Ercan^{1*}, B. Maden^{1*}, S. Kara^{1*}, F. Sunar¹, T. Aysal², N. Ozkaya², O. Saglam²

¹ITU, Civil Engineering Faculty, Geomatics Engineering Department, 80626 Maslak, Istanbul, Turkiye
(ercan18, karas18, madenb17, fsunar) @itu.edu.tr

²Namik Kemal University, Faculty of Agriculture, Tekirdag, Turkiye
(taysal, osaglam, nozkaya) @nku.edu.tr

KEY WORDS: Sunflower fields, Beet webworm moth, Sentinel-2A and PlanetScope, Spectral indexes, Random Forest classification

ABSTRACT:

The diversity of sensors in remote sensing allows for faster and easier detection of changes and issues across different scales, in contrast to conventional ground-based systems. One of the most important distinguishing features among these sensors is their varying resolutions, contributing to the versatility of remote sensing technologies across diverse environmental applications. In this study, the effectiveness of PlanetScope and Sentinel-2 satellite images with different image resolutions in detecting damage caused by a harmful insect (*beet webworm moth - *Loxostege sticticalis**) in sunflower fields in Lüleburgaz district of Kırklareli in the Trace region was evaluated. Damage rates in sunflower fields were analyzed using various spectral indices (Enhanced Vegetation Index and Chlorophyll Index Green) and spectral transformation (Tasseled Cap Greenness) in conjunction with in situ data. Based on the spectral analysis, the satellite image dated 26 July, which showed the most severe damage, was used in the damage assessment analysis. The damaged areas were compared by classifying both satellite images with the Random Forest algorithm. According to the results of the classification accuracy assessment, PlanetScope satellite imagery showed the highest accuracy, with 90% overall accuracy and 84% Kappa statistics, making it a more suitable sensor choice for agricultural applications.

1. INTRODUCTION

In today's globalizing and expanding globe, the agriculture industry is of critical strategic importance. Meeting the food demands of increasing populations, providing food security, and protecting natural resources all raise the importance of the agricultural industry. According to the "OECD-FAO Agricultural Outlook: 2019-2028" report published by the Organization for Economic Cooperation and Development (OECD), the demand for agricultural products is expected to increase by approximately 15% between 2019-2028 due to population growth (OECD, 2023). As a result, it is critical to regularly monitor agricultural productivity and apply risk-mitigation strategies. Failure to do so may have a detrimental influence on food security and natural resource management, particularly in densely populated areas.

Plant stress, climatic conditions, and insect damage can all significantly affect the health of crops in agriculture, and it's crucial to determine the extent of the damage in these cases. Effective pest management, which includes identifying pests and detecting their damage, is essential to minimize their impact (Qin et al., 2003). One effective strategy for managing pests and disease stress is to detect pest damage as soon as possible, as this can prevent the pests from spreading to other fields and causing a widespread invasion. Delayed detection may necessitate the use of chemical methods such as disinfection, which can be costly and harmful to the environment. To address these challenges, several solutions are being developed today to reduce manpower, save time, and keep up to current on real time improvements.

Remote sensing technology is one such solution that offers a wide range of crop monitoring and pest management capabilities. To analyze factors such as the timing, rate, and spread of pest damage to crops, satellite imagery with a variety of properties and resolutions is used in crop monitoring. In agricultural applications, high spatial resolution satellite imagery is preferred over low spatial resolution satellite imagery because heterogeneous (complex) pixels are avoided when obtaining information such as stress and health status of products

through satellite images and distinguishing different situations in damage analysis. The spectral reflectance properties and spectra of different crop types, such as wheat, corn, and sunflowers, exhibit significant differences, highlighting the critical role of high spectral resolution in remote sensing-based crop mapping to differentiate between these crops (Wu et al., 2017). Another significant component is temporal resolution, because it is impossible to analyze the time period when pests start to damage plants without a satellite image of that time period.

Several image transformations can be used to improve the quality of satellite images and extract useful information, which can aid in applications such as land cover classification, environmental monitoring, and disaster assessment. Spectral transformations, such as Vegetation Indices (VIs) and Tasseled Cap (TC) transformations, are commonly used in studies that focus on vegetation analysis. Vegetation Indices (VIs) are designed to amplify sensitivity to vegetation characteristics while mitigating the impact of confounding factors such as soil background reflectance, directional effects, and atmospheric influences. These transformations typically exploit information contained in canopy reflectance or radiance in the red and near infrared (NIR), and are a fundamental part of the analysis of vegetation-related studies (Fang and Liang 2008; Akkartal et. al., 2004; Kara et. al, 2023). On the other hand, TC transformations are used to capture important landscape features by combining the original spectral bands of satellite data linearly into a set of transformed components - Brightness, Greenness and Wetness. This fixed, sensor-specific transformation, based on soil and vegetation signatures, is valuable for characterizing environmental factors in vegetation, emphasizing general plant growth as well as distinct changes in soil moisture, leaf density, and vegetation health (Crist and Cicone, 1984).

The study area, Thrace region, is known for its extensive sunflower production. The *beet webworm moth* (*Loxostege sticticalis*, *Lepidoptera: Pyralidae*) can cause occasional outbreaks during its caterpillar stage. The first documented outbreak in Thrace was in 1975 (Ünal, 1979), with a recurrence in 2012 (Bahadır et al., 2016). This study assesses damage in the

Lüleburgaz region during the 2022 caterpillar outbreak using PlanetScope and Sentinel-2 satellites. Analyzing various spectral indices alongside in-situ data, a Random Forest (RF) algorithm, employing different band combinations, classified the satellite image with the highest pest damage. The results aim to identify the most effective satellite data for accurate detection of *beet webworm moth* damage in sunflower fields and contribute to dynamic agricultural pest management.

2. STUDY AREA

Kırklareli province, located on the European continent, is in the Thrace region of the Marmara Region. It covers an area of 6,459 km² and has an altitude of 203 m (Republic of Türkiye Ministry of Environment and Urbanization, 2023). Kırklareli has a strategically advantageous geographical location as a transitional corridor between the European and Asian continents, which contributes to its high potential in agricultural and animal production. When examining the agricultural land of Kırklareli in terms of crops and production, it is rich in cereals, oilseeds (especially sunflower, which has a high oil content), forage crops and industrial crops. Notably, Kırklareli constitutes the primary sunflower cultivation area in Turkey, contributing to 9.6% of the country's total sunflower production.

Lüleburgaz is the largest settlement in the Kırklareli province, covering a total area of 1370 hectares. The total arable land area is 82,400 hectares, of which 76,600 hectares are cultivated with crops (Lüleburgaz Chamber of Commerce and Industry). As one of the major crops cultivated in this region, Figure 1 illustrates the distribution of sunflower fields in the study area, which includes part of Lüleburgaz.

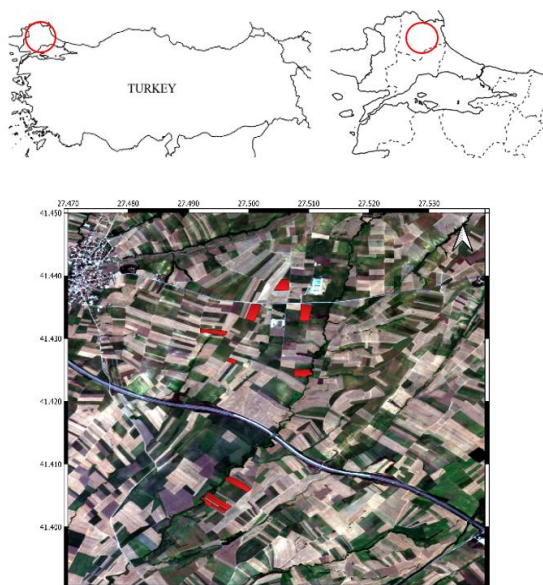


Figure 1. Map of the study area in the Lüleburgaz neighborhood, Kırklareli, showing the locations of 10 in-situ sunflower fields overlaid on the PlanetScope satellite image (© Planet).

3. MATERIALS AND METHODOLOGY

3.1 Materials

In this study, Sentinel-2 (S2) and PlanetScope (PS) images from July 6, July 16, and July 26 were utilized as the satellite dataset. S2 is frequently used in remote sensing applications to understand and monitor changes in land and agricultural conditions due to its 290 km area width and frequent revisit periods (The European Space Agency, 2023). S2 images, which offer different levels of atmospheric correction such as Top of

the Atmosphere (TOA) and Bottom of the Atmosphere (BOA), are available free of charge from the European Space Agency.

The other satellite used in this study, PS, is a constellation of 130 satellites operated by Planet (Planet, 2023). Planet's unique combination of coverage, frequency, and resolution enables the acquisition of information regarding land surface conditions and changes. The main characteristics of the S2 satellite, which has different spatial resolutions (10m, 20m and 60m) at many different wavelengths (Coastal Blue - SWIR) and the main characteristics of the PS satellite, which has high spatial resolution (3m) at many different wavelengths (Green I - Yellow), are shown in the table below (Table 1).

Main features	PS	S2
Spectral resolution		
Spatial resolution	3-m	10-m / 20-m / 60-m
Temporal resolution	Daily	10 days with each satellite five days with (Sentinel 2A & 2B)
Radiometric resolution	8 bytes	12 bytes

Table 1. Comparisons of the PS and S2 satellites' main features (Planet, 2023).

In this study, a dataset comprising 10 sunflower fields was utilized as in-situ data, as detailed in Table 2. This in-situ data includes information such as the percentage of pest damage and the date of the damage measurement. Seven sunflower fields obtained from in-situ data were used for the training dataset, while the remaining three fields were utilized for validation purposes.

Field	Plantation Area	Percentage of Damage	Date of Damage
A	25.95	5	2022/07/29
B	19.20	5	2022/08/02
C	8.52	5	2022/08/02
D	8.05	5	2022/08/02
E	36.99	5	2022/08/01
F	15.50	10	2022/07/29
G	7.95	40	2022/07/29
H	23.99	40	2022/08/01
I	37.84	45	2022/08/01
J	28.58	50	2022/07/29

Table 2. Main features of 10 sunflower fields used in study.

3.2 Methodology

The methodology used in this study consists of two main stages, as shown in the flowchart given in Figure 2. In the first stage, spectral vegetation indices and spectral transformation techniques were used to determine the health status of sunflower fields and to examine the damage caused by pests. In the next stage, in-situ data were regrouped into two classes and image classification was performed using RF algorithm for three classes (Slightly Damaged - Heavily Damaged - Fallow Field) to create a thematic map showing different levels of damaged areas in the study area.

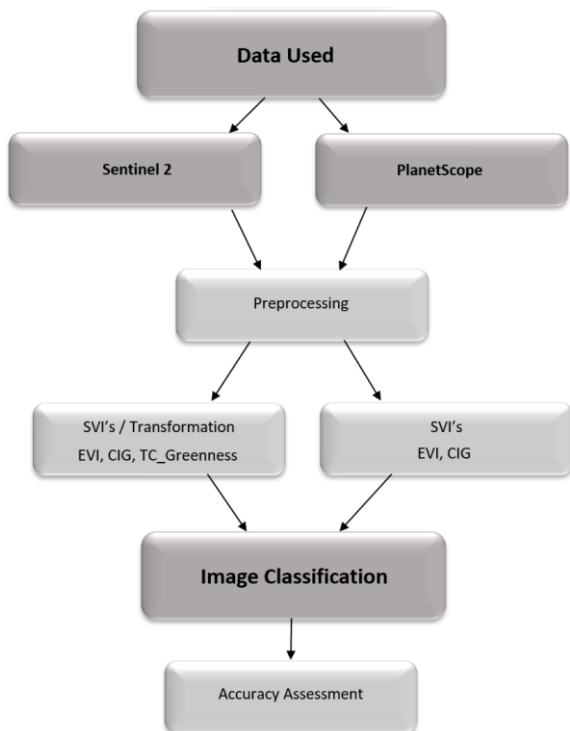


Figure 2. Flowchart of the methodology used.

3.2.1 Spectral Vegetation Index: Various spectral vegetation indices have been developed for agricultural studies. These indices, obtained by calculating reflectance values in two or more spectral bands, provide information about the growth stages of crops (Taşan et al., 2022; Sunar et al., 2011).

The study employed the Enhanced Vegetation Index (EVI) and Chlorophyll Index Green (CIG) as spectral vegetation indices to identify pest damage in sunflower fields and analyze crop health. EVI uses the red, blue and near-infrared bands to account for variations in canopy background reflectance and atmospheric influences, and provides a more accurate estimate of vegetation characteristics, particularly in areas of dense vegetation or under adverse atmospheric conditions (Huete et al., 2002). Given that the CIG is designed for the estimation of chlorophyll content in plants, offering insights into plant vitality, chlorophyll synthesis, and photosynthetic activity, monitoring long or medium-term changes in chlorophyll content within vegetation becomes pivotal for a comprehensive understanding of growth stages and canopy stresses (Niu et al., 2022; Gitelson et al., 2005).

3.2.2. Spectral Transformation: As a spectral transformation, TC, a technique widely used for analyzing and mapping vegetation phenomenology, was applied in this study. Within the generated tasseled cap components, the Greenness component is particularly useful for understanding environmental factors in the field and highlights significant changes in color, leaf density, and plant health, providing valuable insights into both specific issues like pest damage and general plant growth dynamics (Ma et al., 2019).

3.2.3. Image Classification: Image classification is the process of categorizing and labelling groups of pixels in an image according to certain rules. Unsupervised and supervised image classification are the two most common approaches. In this study, the Random Forest, a supervised Machine Learning (ML) algorithm, was used. The main objective is to analyze and interpret the complex patterns and information contained in

images, transforming the raw data into more meaningful information applicable for various environmental purposes, including agricultural monitoring and natural resource management.

3.2.4 Random Forest Algorithm: This algorithm, extensively applied in supervised learning, demonstrates efficacy in both classification and regression analyses within ML. By utilizing ensemble learning, it integrates multiple classifiers to enhance the overall performance of the model (IBM, 2023; Sunar et al., 2017). This algorithm comprises a substantial number of decision trees collaborating as a community, yielding effective classification results through the creation of multiple independent trees. The ultimate prediction arises from a majority vote, wherein the class attaining the highest number of votes becomes the model's prediction.

4. APPLICATION AND RESULTS

The *beet webworm moth*, scientifically described by Carl Linnaeus in 1761, is a widespread pest found across Asia, Europe, North America, and the Arabian Peninsula (Kuznetsova and Chumakov, 2008). In Turkey, it is distributed in various provinces, including Amasya, Antalya, Balıkesir, Bitlis, Bursa, Çanakkale, Düzce, Istanbul, Kırklareli, Konya, Malatya, and Kahramanmaraş (Öztemiz and Ciner, 2022). This moth species, known to feed on approximately 200 different plant species, is recognized as a pest affecting cereals, oilseeds, legumes, fiber crops, and vegetables (Alekhin and Kuznetsova, 2003). It causes significant damage in agricultural areas, particularly on economically vital crops such as soybeans, sugar beet, alfalfa, and sunflower (Feng et al., 2004; Xiao et al., 2008).

Pests typically cause damage to plant leaves, hindering growth by creating small holes in young plants, as illustrated in Figure 3. Furthermore, they can impact the reproductive organs of the plant, damaging flower buds and immature fruits. This situation was experienced during the growth process of sunflower plant in the study area and negatively affected the harvest productivity.



Figure 3. Leaf damage caused by *beet webworm moths*.

As an initial step, spectral reflectance profiles were extracted from the multitemporal dataset to distinguish between slightly and significantly damaged sunflower fields, and their spectra are presented in Figure 4. Owing to the distinct spectral resolutions of the PS and S2 satellites, noticeable differences exist in the spectral reflectance curves. As clearly seen, the higher spectral resolution of the S2 image, indicated by the higher number of bands, allows a more continuous spectral profile to be generated, allowing for more accurate spectral analysis.

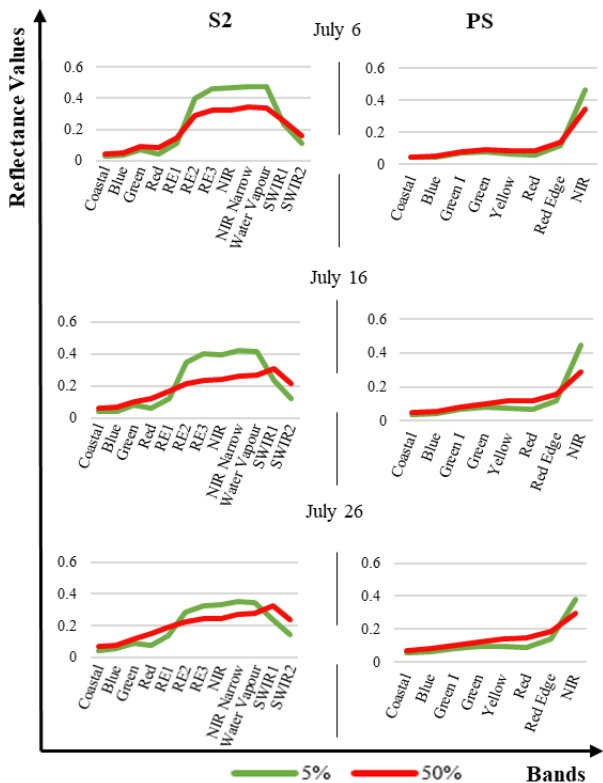


Figure 4. Reflectance spectra of slightly and significantly damaged sunflower fields.

A close examination of the spectral curves of the sunflower fields shows that the 5% damaged sunflower field has a typical spectral curve for a healthy sunflower crop on 6 July and 16 July, with some changes in reflectance on 26 July. Despite July being the growing month for sunflower fields, on 26 July, it was noted that the spectral reflectance values of the 5% damaged field in the Red - Red Edge and NIR bands were similar to those of the 50% damaged field, deviating from the typical healthy plant spectral curve (i.e., decrease from 0.5 to less than 0.4). This change in vegetation health can also be seen between the PS 6 - 26 July spectral curves. In contrast, the 50% damaged field has a significantly lower reflectance in the NIR band than the 5% damaged field for both satellites. In particular, examination of the S2 spectral curves on 16 and 26 July reveals a different trend in the spectral curve of the 50% damaged field compared to that of a typical healthy crop.

The analysis of spectral curves in PS highlights the challenge of distinguishing between slightly and significantly damaged fields. This difficulty is primarily due to the low spectral resolution in the VIS-NIR region. In other words, the higher spectral resolution of the S2 sensor with a greater number and narrower Red Edge and NIR bandwidth clearly demonstrates that it is a more suitable sensor for discriminating vegetation health and providing more accurate spectral analysis.

In the subsequent phase, two spectral vegetation indices (EVI and CIG) along with TC-Greenness were applied to all S2 and PS images using the Google Earth Engine platform. Figure 5 shows the spectral index values for ten fields and emphasizes the temporal variation of insect damage to biomass.

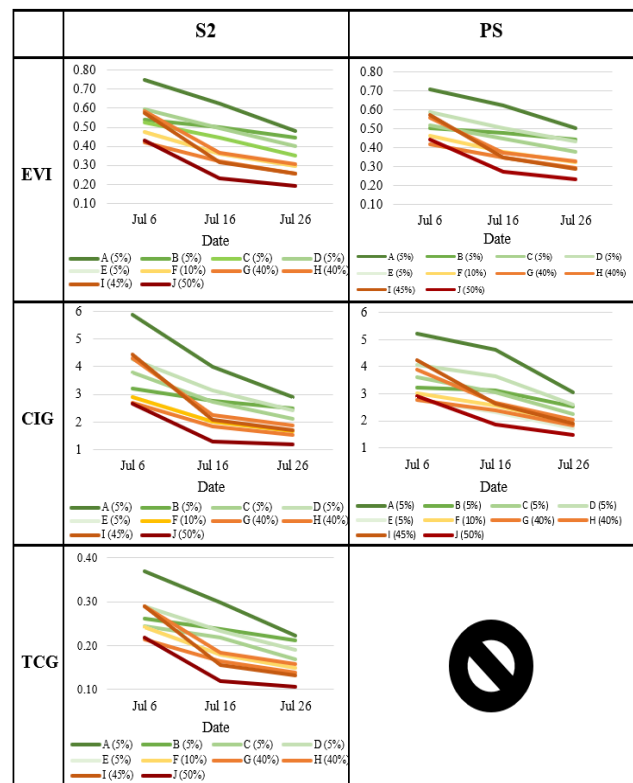


Figure 5. Comparison of multitemporal EVI, CIG and TC-Greenness profiles for ten sunflower fields.

When examining the graphs in Figure 5, a notable decrease is observed in both the spectral index and TC Greenness values for all fields from July 6 to July 26. Additionally, it is observed that the S2 and PS satellite systems show similar EVI values across all fields. However, this trend is not observed in CIG values, especially on July 16. For instance, the CIG index value for the S2 satellite of Field A decreases from 6 on July 6 to 4 on July 16. In contrast, for the PS satellite of the same field, CIG values remained relatively consistent, staying around 5 on both days. Similar variations are noted in all slightly damaged fields, while this pattern is consistent for both satellites in significantly damaged fields.

When examining the TC-Greenness component, as illustrated in Figure 5, it is important to note that this component could not be calculated for the PS dataset due to the absence of sensor-dependent coefficients required for this transformation. However, in general, it is observed that the TC-Greenness graph obtained with S2 is similar to the S2 EVI.

Given the similarity in spectral profiles among fields with comparable damage areas, it was considered more appropriate to categorize the in-situ data into two primary classes: slightly damaged areas (damage classes A to F in Table 2) and significantly damaged areas (damage classes G to J in Table 2). This reclassification enhances the clarity of rapidly detecting damage in the area and identifying the peak damage periods. In other words, to more accurately evaluate and compare these two main damage classes, two spectral indexes and TC-Greenness transformations were applied to both S2 and PS satellite images, and the results are presented in Figure 6.

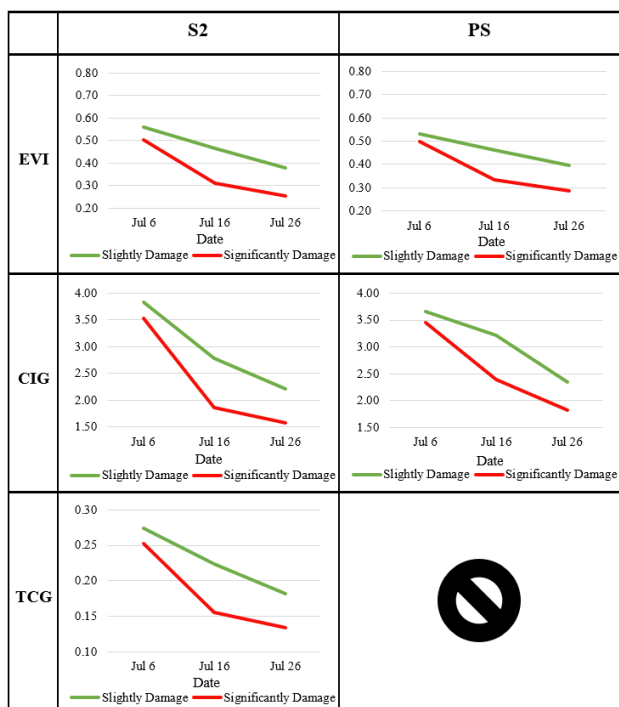


Figure 6. Comparison of multitemporal EVI, CIG and TCG profiles for 2 main (slightly and significantly) damaged classes.

Comparing the spectral index and transformation graphs presented in Figure 6, temporal differences become evident, indicating a decreasing trend for the two main damage groups in both datasets. These graphs offer valuable insights into the initiation and progression of damage. Specifically, on July 6, the index values for slightly damaged and significantly damaged classes were closely aligned. However, a sudden decrease in the index values of the significantly damaged class on July 16 indicates a decline in plant health. This decrease provides evidence of deterioration attributed to pest damage. The decreasing trend persists, signifying ongoing damage caused by pests and leading to the identification of the period between July 16 and July 26 as the initiation of damage. In a final assessment, July 26 is pinpointed as the date when pest damage reaches its peak, aligning with the date recorded in in-situ measurements and interviews with farmers.

As the final step, images taken on July 26, determined as the peak of damage, were classified using the RF algorithm, resulting in the creation of a damage thematic map for the study area. The classification process considered three main classes: slightly damaged sunflower fields, significantly damaged sunflower fields, and fallow fields characterized by abundant bare soil (open field). Various scenarios were explored during this step, incorporating not only the original bands but also spectral indices, transformed component, and/or their combinations in the classification process. Table 3 displays the classification output images generated under various scenarios.

Visual analysis of the classification results reveals that the fields situated at the top of the road exhibit more severe damage compared to those at the bottom. Additionally, in the majority of output images from the classification scenarios, the visual analysis indicates a higher presence of the significantly damaged class in the PS outputs compared to the S2 outputs.

Another visual analysis result indicates that field boundaries are more easily detected in the output images from the PS satellite

system, owing to its higher spatial resolution compared to the S2 satellite images.

The classification results should undergo not only visual analysis but also quantitative assessment using an error matrix. Table 4 presents the calculated overall accuracy and Kappa statistics for each classification. Upon examining the accuracy measurements, it was observed that higher accuracies were achieved when excluding the Coastal band (B₁) in the classifications for both satellites. Consequently, the B₁ band was not considered in other scenarios.

	S2	PS
All Bands		
All Bands-B1		
(All Bands-B1)+EVI		
(All Bands-B1)+CIG		
(All Bands-B1)+EVI, CIG		
Legend		
Slightly Damage	Significantly Damage	Fallow Land

Table 3. Classification output images for various scenarios on the most damaged date (July 26th).

As presented in Table 3 and Table 4, visual and quantitative differences in the results arise between the two satellite images, attributed to variations in their spatial and spectral resolutions. The use of different combinations of two indices/component, instead of employing all indices/component in the classification process, has been observed to positively impact accuracy. As indicated in Table 4, the best scenarios selected were not the same between the two satellite images, owing to their varying image resolutions.

		Overall Accuracy	Kappa Accuracy
S2	All Bands	0.78	0.63
	All Bands – B ₁	0.81	0.70
	(All Bands – B ₁) + EVI	0.81	0.68
	(All Bands – B ₁) + CIG	0.82	0.71
	(All Bands – B ₁) + TCG	0.79	0.66
	(All Bands – B ₁) + EVI, CIG	0.83	0.72
	(All Bands – B₁) + EVI, TCG	0.84	0.73
	(All Bands – B ₁) + CIG, TCG	0.77	0.62
	(All Bands – B ₁) + EVI, CIG, TCG	0.81	0.72
	PS	All Bands	0.75
All Bands – B ₁		0.88	0.79
(All Bands – B ₁) + EVI		0.85	0.75
(All Bands – B₁) + CIG		0.90	0.84
(All Bands – B ₁) + EVI, CIG		0.88	0.80

Table 4. Accuracy assessments for various classification scenarios, including overall accuracy and Kappa statistics.

Specifically, the best result obtained from the classification of PS satellite images is a 90% overall accuracy using (All Bands - B₁) + CIG classification. In contrast, this scenario does not yield the highest accuracy (i.e., 82%) for S2 classified images. The highest accuracy result for S2 is achieved with (All Bands - B₁) + EVI, TCG classification with 84% Overall accuracy. In this context, this raises the question of whether it would have been possible to achieve higher than 90% overall accuracy with this classification for PS if TCG coefficients had been determined for PS.

The computed areas for each of the three classes from the scenario that yields the highest classification accuracy for both S2 and PS are presented in Table 5. When comparing the areas of the classes in Table 5, the most notable difference is observed in the significantly damaged class. This discrepancy can be

attributed to variations in sunflower planting dates across the region, indicating that the chosen date for image classification (i.e., July 26) may not be representative of the entire area. Given that the choice of the July 26 date is consistent with existing in situ data, the need for more comprehensive in situ and ancillary data is underlined. This is crucial not only for accurately determining the optimum date indicating damage, but also for all processing stages.

Fields	S2	PS	Δ
Slightly damaged (decare)	9187.3	8655.3	532
Significantly damaged (decare)	12426.6	14479.2	2052.6
Fallow land (decare)	3726.7	2203.5	1523.2

Table 5. Comparison of the computed areas for main classes in highest accuracy scenario.

5. CONCLUSION

This study was initiated to evaluate the infestation of *beet webworm moths* in sunflower fields in Lüleburgaz in 2022 using remote sensing techniques and to determine varying degrees of damage in the fields. To achieve this, in-situ data was collected from specific fields and accurate damage assessments were made through various image processing analyses, including vegetation indices and machine learning-based image classification.

Despite the limitations in accuracy assessment due to the small number of available in-situ data, overall accuracy for different classification scenarios, evaluating the contribution of spectral indices and transformations to image classification, ranged from a minimum of 75% to a maximum of 90%. Due to differences in image resolutions, particularly spectral and spatial, between the two satellite systems (and the inability to determine TC-Greenness coefficients for PS), the most accurate classification scenarios varied. PS achieved 90% overall accuracy with (All Bands - B₁) + CIG classification, while S2 achieved 84% overall accuracy with (All Bands - B₁) + EVI, TC-Greenness classification.

The study's findings highlight the significant contribution of remote sensing technology in detecting temporal changes in pest damage during the growth stages of agricultural products and subsequently determining damage rates. This not only aids decision-making authorities in taking necessary precautions but also provides better opportunities for effective agricultural management.

REFERENCES

- Akkartal, A., Türüdü, O., Erbek Sunar, F., 2004. Analysis of Changes in Vegetation Biomass Using Multitemporal and Multisensor Satellite Data. In *XXXV ISPRS Congress* (pp. 12-23).
- Alekhin, V.T., Kuznetsova, T.L., 2003. The Beet Webworm and Control Measures Against It (Recommendations). *FGNU Rosinformagrotek*, Moscow, pp.76.
- Bahadır, F., Işık, N., Bulut, E., Alagöz, V., Sağlam, Ö., 2016. The Legendary Pest Returns in the Thrace Region: Sunflower Meadow Moth *Loxostege sticticalis* L. (Lep. Pyralidae). (In Turkish), *6th National Agriculture Student Congress*, 4-6 May, Ankara.

- Crist, E.P., Cicone, R.C., 1984. Application of the Tasseled Cap Concept to Simulated Thematic Mapper Data. *Photogrammetric Engineering and Remote Sensing*, 50(3), 343-352.
- ESA, 2023. Sentinel-2 Operations
https://www.esa.int/Enabling_Support/Operations/Sentinel_2_operations (Accessed Oct 30, 2023)
- Fang, H., Liang, S., 2008. Leaf Area Index Models. Encyclopedia of ecology, five-volume set.
- Feng, H., Wu, K., Cheng, D., Guo, Y., 2004. Spring Migration and Summer Dispersal of *Loxostege Sticticalis*. (Lepidoptera: Pyralidae) and Other Insects Observed With Radar in Northern China. *Environmental Entomology*, 33 (5), 1253-1265.
- Gitelson, A.A., Viña, A., Ciganda, V., Rundquist, D.C., Arkebauer, T.J., 2005. Remote Estimation of Canopy Chlorophyll Content in Crops. *Geophysical Research Letters*, 32(8).
- Huete, A., Didan, K., Miura, T., Rodriguez, E.P., Gao, X., Ferreira, L.G., 2002. Overview of the Radiometric and Biophysical Performance of the MODIS Vegetation Indices. *Remote Sensing of Environment*, 83(1-2), 195-213.
- IBM, 2023. What Is Random Forest?
<https://www.ibm.com/topics/random-forest#:~:text=Random%20forest%20is%20a%20commonly,both%20classification%20and%20regression%20problems>. (Accessed Oct 30, 2023)
- Kara, S., Maden, B., Ercan, B.S., Sunar, F., Aysal, T., Saglam, O., 2023. Assessing the Impact of Beet Webworm Moths on Sunflower Fields Using Multitemporal SENTINEL-2 Satellite Imagery and Vegetation Indices. The International Archives of the Photogrammetry, Remote Sensing and Spatial Information Sciences, 48, pp.521-527.
- Kuznetsova, T.L., Chumakov, M.A., 2008. *Loxostege Sticticalis* L.-the Beet Webworm, In: Interactive Agricultural Ecological Atlas of Russia and Neighboring Countries. Economic Plants and their Diseases, Pests and Weeds (Ed. Afonin AN, Greene SL, Dzyubenko NI, Frolov AN) form <http://www.agroatlas.ru/en/content/pests/Loxostegesticticalis>
- Luleburgaz Chamber of Commerce and Industry, 2023. Luleburgaz region, <https://www.ltso.org.tr/bolge-hakkinda> (Accessed Oct 25, 2023)
- Ma, H., Huang, W., Jing, Y., Yang, C., Han, L., Dong, Y., Ye, H., Shi, Y., Zheng, Q., Liu, L., Ruan, C., 2019. Integrating Growth and Environmental Parameters to Discriminate Powdery Mildew and Aphid of Winter Wheat Using Bi-temporal Landsat-8 Imagery. *Remote Sensing*, 11(7), 846.
- Niu, H., Wang, D., Ehsani R., Chen, Y., 2022. Tree-level Yield Estimation Using UAV-based Vegetation Indices and Plant Physiology-informed Machine Learning, 2022 *International Conference on Unmanned Aircraft Systems (ICUAS)*, Dubrovnik, Croatia, 1614-1619.
- OECD, 2023. OECD-FAO Agricultural Outlook 2019-2028, <https://www.oecd.org/agriculture/oecd-fao-agricultural-outlook-2019/> (Accessed May 14, 2023).
- Öztemiz, S., Ciner, İ., 2022. Climate Change Caused the Outbreak of First Generation Butterflies of Meadow Caterpillar (*Loxostege Sticticalis* L.) in Düzce [in Turkish]. *Düzce University Journal of Science and Technology*, 10(3), 1398-1407.
- Qin, Z., Zhang, M., Christensen, T., Li, W., Tang, H., 2003. Remote Sensing Analysis of Rice Disease Stresses for Farm Pest Management Using Wide-band Airborne Data. In *IGARSS 2003. 2003 IEEE International Geoscience and Remote Sensing Symposium. Proceedings (IEEE Cat. No. 03CH37477)*, Vol. 4, pp.2215-2217.
- Planet, 2023. Planet Imagery Product Specifications.
https://assets.planet.com/docs/Planet_Combined_Imagery_Product_Specs_letter_screen.pdf (Accessed April 1, 2023)
- Republic of Türkiye Ministry of Environment and Urbanization, 2023. <https://kirkclareli.csb.gov.tr/genel-bilgiler-i-3772> (Accessed Oct 25, 2023)
- Sunar, F., Özkan, C., Osmanoglu, B., 2011. Remote Sensing [Uzaktan Algılama; in Turkish], Anadolu University Press, (No. 2320/1317).
- Sunar, F., Ozkan, C., Ok, A.O., Osmanoglu, B., Avci, Z.D.U., Berberoglu, S., 2017. Digital Image Processing [Dijital Görüntü İşleme; in Turkish], Anadolu University Press, ISBN: 978-975-06-2265-6.
- Taşan, S., Cemek, B., Taşan, M., Cantürk, A., 2022. Estimation of Eggplant Yield with Machine Learning Methods Using Spectral Vegetation Indices. *Computers and Electronics in Agriculture*, 202, 107367.
- Ünal, E., 1979. Research on the Identification, Bio-ecology and Control Methods of Meadow Caterpillar (*Loxostege sticticalis* L.) Damaging Sunflowers in Marmara Region. [in Turkish]. A107.017 No. Project Work Report. Regional Agricultural Control Research Institute-Istanbul.
- Wu, M., Huang, W., Niu, Z., Wang, Y., Wang, C., Li, W., Hao P., Yu, B., 2017. Fine Crop Mapping by Combining High Spectral and High Spatial Resolution Remote Sensing Data in Complex Heterogeneous Areas. *Computers and Electronics in Agriculture*, Vol. 139, pp.1-9.
- Xiao, C., Baoping, Z., Ruijie, G., Minghao, Y., You, Z., Kuijun, Z., 2008. Source Area of Spring Population of Meadow Moth, *Loxostege Sticticalis* L. (Lepidoptera: Pyralidae), in Northeast China. *Acta Ecologica Sinica*, 28 (4), 1521- 1535.